PNAS RESEARCH ARTICLE | BIOPHYSICS AND COMPUTATIONAL BIOLOGY OPEN ACCESS

Evidence for a possible quantum effect on the formation of lithium-doped amorphous calcium phosphate from solution

Joshua S. Straub[a,1], Manisha L. Patel[a,1], Mesopotamia S. Nowotarski[b], Lokeswara Rao[b], Mark E. Turiansky[c], Matthew P. A. Fisher[a,2], and Matthew E. Helgeson[d,2]

Affiliations are included on p. 7.

Contributed by Matthew P. A. Fisher; received November 8, 2024; accepted January 29, 2025; reviewed by Leo Radzihovsky and Jeffrey D. Rimer

Differential isotope effects are an emerging tool for discovering possible nontrivial quantum mechanical effects within biological systems. However, it is often nearly impossible to elucidate the exact mechanisms by which a biological isotope effect manifests due to the complexity of these systems. As such, one proposed in vitro system of study for a quantum isotope effect is calcium phosphate aggregation, where symmetric calcium phosphate molecular species, known as Posner molecules, have been theorized to have phosphorus nuclear spin–dependent self-binding rates, which could be differently modulated by doping with stable lithium isotopes. Here, we present in vitro evidence for such a differential lithium isotope effect on the formation and aggregation of amorphous calcium phosphate from solution under certain conditions. Experiments confirm that lithium incorporates into amorphous calcium phosphate, with ^{7}Li found to promote a greater abundance of observable calcium phosphate particles than ^{6}Li under identical solution preparations. These in vitro results offer a potential explanation for in vivo biological studies that have shown differential lithium isotope effects. Given the importance of calcium phosphate in biological systems—ranging from mitochondrial signaling pathways to key biomineralization processes, as well as the proposed role of Posner molecules as a "neural qutrit"—these results present an important step in understanding calcium phosphate nucleation as well as the potential role of calcium phosphate for quantum biology and processing.

quantum biology | quantum brain theory | calcium phosphate | biomineralization

Over the past decade, there has been growing interest in the area of "quantum biology," where quantum mechanics is theorized to be nontrivially functional in a variety of biological systems. Evidence of quantum biological effects exists in a number of systems including proton tunneling in proteins (1, 2), olfaction (3), photosynthesis (4–6), and magnetoreception in birds (7–9). However, experimentally confirming or discovering cases of quantum biological effects is a significant challenge, as the warm, crowded environments found in biology are juxtaposed to the cold, isolated environments favorable for discovering and understanding quantum mechanical behavior. One area of interest within quantum biology is spin-based effects, ranging from singlet-triplet conversion in electron spin pairs to nuclear spin information storage (4, 10). Differential isotope effects offer a useful strategy for identifying spin-mediated cases of quantum biology, as the isotopes can have different spin–spin interactions but similar chemical interactions. Recently, a number of biological isotope effects have been discovered which cannot be readily explained by the classical mass-based kinetic isotope effect, including lithium isotope effects on mothering behavior (11) and the suppression of mania (12) in rats, a xenon isotope effect on xenon's anesthetic properties in mice (13), and recently, a lithium isotope effect on mitochondrial calcium sequestration (14). However, due to the complex nature of biological systems, it is almost impossible to definitively place the origins of these isotope effects. Recently, experimental tests of Li isotope effects on key neuronal and enzymatic activities found no distinguishable differences (15) that link the observed effects to differential uptake into cells. While the radical pair mechanism has been proposed for both xenon anesthesia and lithium mania suppression (16, 17), such modeling efforts are speculative in that they fail to link the spin dynamics to any biological function that would impact the observed behavior. As a result, to build a greater understanding of quantum effects in biological systems, it is important to find in vitro systems that demonstrate such nonclassical isotope effects so that these quantum effects can be investigated in a systematic manner.

Significance

The warm-and-wet environment of biology is traditionally thought to be inhospitable to quantum effects. However, this study reports the identification of potential nonclassical quantum effects in a model for in vitro biomineralization. Specifically, we observe that lithium isotopes differentially alter mesoscale calcium phosphate mineralization in common biologically relevant aqueous solutions. This isotope effect is entirely unexpected from classical chemistry principles but is well predicted by quantum dynamical selection—the mechanism underpinning an existing theory for calcium phosphate–mediated quantum processing. The finding that lithium alters the formation of calcium phosphate in an isotope-dependent manner may be key to understanding lithium's role in living systems, including a number of previously observed but poorly understood effects in biological models of lithium therapy.

Reviewers: L.R., University of Colorado, Boulder; and J.D.R., University of Houston.

The authors declare no competing interest.

[1]J.S.S. and M.L.P. contributed equally to this work.

[2]To whom correspondence may be addressed. Email: mpaf@ucsb.edu or helgeson@ucsb.edu.

This article contains supporting information online at https://www.pnas.org/lookup/suppl/doi:10.1073/pnas.2423211122/-/DCSupplemental.

Published March 6, 2025.

Given the prevalence of apparent lithium isotope effects across a range of biological functions, one broad context to search for such a system considers the formation and aggregation of calcium phosphate. Calcium phosphate mineralization is important in a wide range of biological contexts, including the formation of hydroxyapatite in teeth and bone (18, 19), and in mitochondrial pathways, where amorphous calcium phosphate granules act as biological stores of calcium and phosphate ions (20, 21). In addition, calcium phosphate biomineralization has been implicated in a number of disease conditions, including brushite crystallization in human kidney stones (22, 23) and hydroxyapatite formation in atherosclerosis tissue (24, 25). Lithium has also been proposed to incorporate into calcium phosphate nanoclusters and impact their binding dynamics in an isotope-dependent manner (10, 26, 27). Moreover, in medicine, lithium has been implicated in the decalcification of teeth as an unwanted side-effect of lithium-based treatments (28), suggesting that lithium may affect the aggregation and/or stability of calcium phosphate. Thus, the calcium–phosphate–lithium system provides an in vitro model with interesting potential for elucidation of possible quantum effects in biological systems.

Recent advances in our understanding of the early stages of calcium phosphate mineralization from solution have confirmed the existence of molecular clusters which provide a novel route of nucleation and aggregation (29–31). While the exact stoichiometry and structure of these calcium phosphate molecular species are still unknown, the two primary proposals are as follows: 1) Some form of ionic calcium triphosphate (such as $[Ca(H_2PO_4)_{1.04})(HPO_4)_{1.76}]^{2.56-}$) (30, 32), and 2) the Posner molecule ($Ca_9(PO_4)_6$) (29, 33, 34). It is also conceivable that these two proposed molecular clusters can exist in equilibrium. The latest understanding of calcium phosphate nucleation and aggregation based on these molecular species is shown in Fig. 1 (29, 30, 35–38). Before calcium phosphate nucleation, phosphate ions are in exchange with phosphate assemblies, liquid-like clusters of phosphates that form in aqueous solution (37) (stage I). Solution conditions such as ion concentration, temperature, and pH then encourage the formation of molecular clusters from soluble ions (stage II), which nucleate into nanocolloids of amorphous calcium phosphate (ACP) (stage III). These ACP nanocolloids then aggregate into larger ACP colloids (29) (stage IV) and in time (minutes to hours depending on solution conditions) undergo phase transformation into crystalline hydroxyapatite, the thermodynamically favored phase (31, 39).

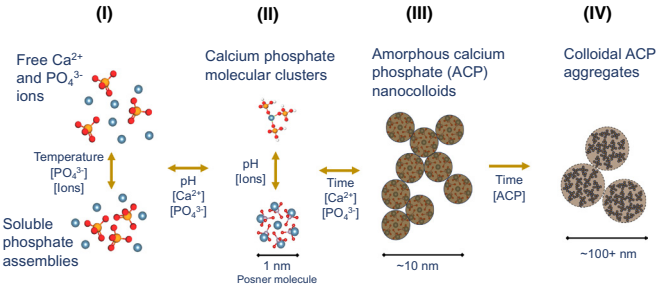

Fig. 1. Proposed nucleation and aggregation pathway for the formation of amorphous calcium phosphate (ACP), showing four proposed stages and the transitions between them. Soluble calcium and phosphate ions (I) initially form molecular clusters (II), which then rapidly form amorphous calcium phosphate (ACP) nanocolloids at 50 to 100 nm in diameter (III). These ACP nanocolloids then aggregate into larger colloidal structures at several hundred nanometers in size (IV). Over time, these metastable ACP aggregates undergo phase transformation to hydroxyapatite.

Within the field of quantum biology, the Posner molecule is of keen interest because of its putative role in the Posner-mediated quantum brain theory (10, 27). This theory proposes that the Posner molecule could function as a biological qutrit in a quantum information network that operates alongside a classical biochemical information network in the mammalian brain. Within the framework of this theory, it is posited that one might observe a differential lithium isotope effect on the aggregation of Posner molecules (27). Previous density functional theory calculations revealed energetic favorability for two Li-ions to replace the central calcium ion in a Posner molecule (26). In such a case, an isotope effect could arise from different couplings between the spin of the two lithium isotopes, ^{6}Li and ^{7}Li, and the ^{31}P spin states within the Posner molecules. Since the collective ^{31}P spin states are proposed to be linked to binding rates of Posner molecules (26, 27), such an isotope effect may manifest on larger scales by altering the aggregation of Posner molecules into larger calcium phosphate species. In biologically relevant conditions, it would be expected that the metastable phase ACP—sometimes described as a "glass" of Posner molecules (33, 40, 41)—would be formed by such initial aggregation events, and thus ACP aggregation could display isotope-dependent kinetics. Given that ^{6}Li and ^{7}Li have identical electronic states, and thus chemistries, and that their diffusion rates in water have been measured to be indistinguishable (42), any observable lithium isotope effect on ACP aggregation would be classically unexpected by the kinetic isotope effect.

Here, we present results that show a measurable differential lithium isotope effect on the in vitro formation of ACP in aqueous solutions that are mildly supersaturated with respect to calcium phosphate. Dynamic light scattering (DLS) measurements of ACP aggregation in the presence of ^{6}Li and ^{7}Li salts at biologically relevant pH and temperature reveal that, while the size of ACP particles is isotope-independent, the concentration of large ACP particles is enriched in the presence of ^{7}Li relative to ^{6}Li. ^{31}P NMR and mass spectrometry directly confirm lithium incorporation into ACP and show significant Li–P spin coupling. Given the biological importance of calcium and phosphate regulation, in several established biological processes as well as the quantum brain theory, these results could have wide implications for the interpretation of the milieu of differential lithium isotope effects that have been previously observed.

DLS Shows Differential Lithium Isotope Effect

DLS allows for the measurement of particle sizes in solution, ranging from 1 nm to several microns in diameter, and has previously been used to measure calcium phosphate structures both at molecular stages (Fig. 1, II) (34, 43) and of larger colloidal structures (Fig. 1, III and IV). (44, 45) Here, we used DLS to monitor the size and scattering intensity of calcium phosphate in solutions promoting ACP formation during the first 5 min of aggregation, as monitored in 10 s intervals. A schematic for the preparation and measurement of these solutions is shown in *SI Appendix*, Fig. S1. Solutions were prepared with 250 mM LiCl (either 95% ^{6}Li or 99% ^{7}Li), 2 mM sodium phosphate, and 5 mM $CaCl_2$ at pHs of 7 to 9 (before calcium) and at 37 °C, which is a similar composition to previous studies, although these were done at 25 °C. These specific conditions were chosen due to their biological relevance to the mitochondrial matrix (noting that the pH drops after calcium addition to the 7 to 8 range), given the mitochondria's importance in buffering intracellular calcium via storage in amorphous calcium phosphate (20, 21), and as a potential location of Posner molecules within the

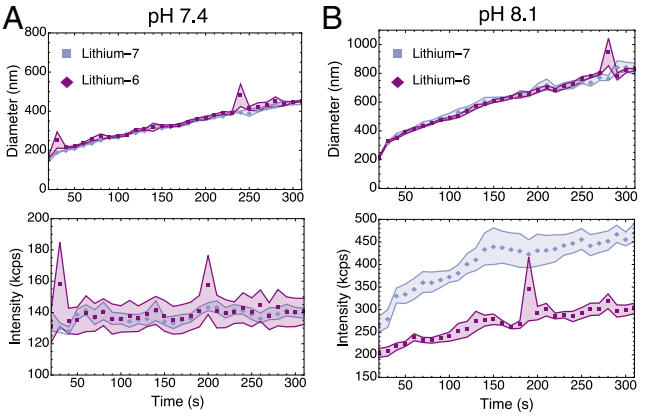

Fig. 2. Dynamic scattering results of the first 5 min of ACP aggregation for a system of 5 mM $CaCl_2$, 2 mM $NaPO_4$, and 250 mM LiCl at 37 °C comparing ^{7}Li and ^{6}Li. (*A*) At pH 7.4, the sizes of calcium phosphate particles and their scattering intensities are the same, indicating no isotopic difference. (*B*) At pH 8.1, the sizes of calcium phosphate are the same, but the ^{7}Li solution shows greater scattering intensity, indicating a higher particle abundance of structures at large sizes. Each trace is the average result over 5 separate trials, with bands indicating the SEM. The pH was adjusted to the indicated value before calcium addition using 0.2 M NaOH.

quantum brain theory. Note that while the solution conditions explored herein are supersaturated with respect to calcium phosphate crystals (46), the solid phase transformation of ACP into hydroxyapatite crystals takes place on a significantly longer timescale than that of these experiments. Thus, we assert that the particles measured via DLS are colloidal ACP aggregates (shown pictographically in Fig. 1, Stage IV). Moreover, X-ray diffraction experiments performed on similarly prepared solutions confirm the identity of ACP (47).

Prior to calcium addition, the solutions were filtered using 0.2 μm cellulose acetate syringe filters and measured for 120 s in DLS to confirm the absence of large contaminant particles. After adding calcium, the average sizes and scattering intensities were measured over a 5-min interval (Fig. 2). At both pH 7.4 and 8.1, the sizes of ACP measured in the presence of the two lithium isotopes were identical. At the lower pH of 7.4, the scattering intensities are also isotope-independent, but at pH 8.1 the scattering intensity in the presence of ^{7}Li is significantly higher, potentially indicating a lithium isotope dependence on the formation of ACP from solution.

To understand the significance of the different scattering intensities despite the similar average particle sizes between solutions containing the two different lithium isotopes, one can consider how scattering intensity scales with particle size and concentration. Drawing from previous observation (45), we consider the wide size dispersity of ACP particles, ranging from molecular clusters at the single nanometer scale to larger ACP colloids (Fig. 1, stages II–IV). Mie scattering theory (*SI Appendix*, Fig. S2) shows that, for particle sizes with diameters above the Rayleigh regime (i.e., having diameter $d > \lambda$, where λ is the wavelength of incident light, in this case, 532 nm), the scattering intensity I scales approximately as $I \propto d^2$ (48), while in the Rayleigh regime ($d \ll \lambda$), the scattering intensity drops significantly, with intensity $I \propto d^6$ (49). Thus, particles at smaller length scales (1 to 10 nm in diameter) will have negligible contribution to the total scattering intensity compared to the largest ACP particles (at several hundred nanometers in diameter).

Considering this size–intensity relationship, one can then extract information on the distribution of particle sizes within the solutions containing each lithium isotope. Given that the cumulant average size is identical for both isotopes, it appears that the largest particles, which dominate the scattering signal, are forming at the same size in the presence of both isotopes. Therefore, the noted difference in scattering intensity can be attributed predominately to the abundance (concentration) of these largest particles, indicating that the ^{7}Li solution has a more concentrated population of large particles. Note that since ^{6}Li and ^{7}Li have indistinguishable aqueous diffusion rates, there should be near identical local ordering of water and therefore solvent occlusion into calcium phosphates formed in the presence of each isotope, so that isotopic impact on scattering length density is expected. Given that the total molar concentrations of calcium and phosphate are identical, the ^{6}Li solution must have a more concentrated population of smaller ACP particles, molecular species, and/or ionic phosphate and calcium, which contribute minimally to the scattering signal, leading to the observed intensity difference.

To further explore this apparent dependence of ACP formation on lithium isotopes, we explored the solution phase behavior of the LiCl–$NaPO_4$–$CaCl_2$ system to test whether the location of the phase boundaries is isotope-dependent. First, the solid-solution phase boundary was measured in pH and [Ca^{2+}] phase space at fixed [PO_4^{3-}]. 35-min absorbance measurements at 532 nm identified three distinct regions—a dissolved free ion phase, a metastable colloidal phase, where calcium phosphate particles formed and exhibited time-insensitive absorbance, and an unstable agglomeration phase, where absorbance traces steadily increase and ACP precipitation occurred within 45 min (*SI Appendix*, Fig. S4). The results (Fig. 3*A*) indicate no isotopic dependence on the location of these phase boundaries.

We then monitored ACP aggregation using DLS at a range of pH within the unstable agglomeration phase to search for the conditions where this isotope effect is present. We find (Fig. 3*B*) that the lithium isotope effect manifests in a specific range of

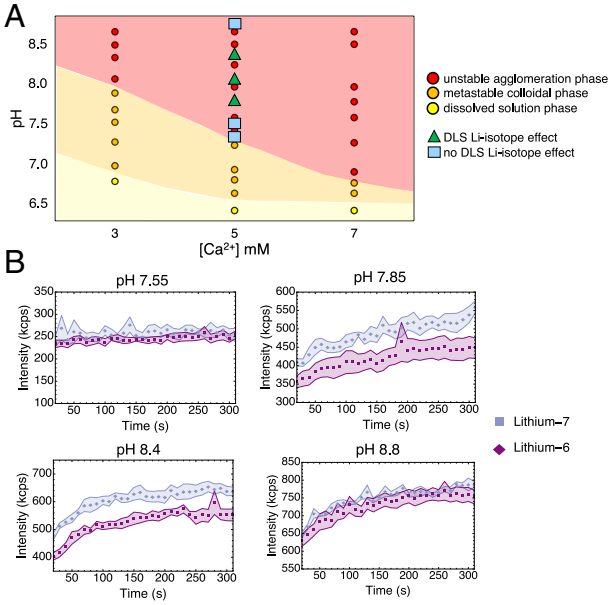

Fig. 3. The solution phase behavior of calcium phosphate shows a specific region of active lithium isotope effect. (*A*) A phase diagram as a function of pH and calcium concentration reveals three distinct regions of ACP aggregation: 1) dissolved free ions, 2) metastable colloidal aggregates, and 3) unstable agglomeration of particles. No isotope difference is found in the location of the boundaries between these regions. (*B*) Exploring pH within the unstable agglomeration phase reveals a distinct pH window where the lithium isotope effect on DLS intensity on ACP aggregation is observable. All samples had identical sizes from DLS, as shown in *SI Appendix*, Fig. S3.

supersaturation, whereas solutions too close to the agglomeration boundary or at too high of a supersaturation show little or no scattering intensity differential. This narrow window indicates that there may be a specific nucleation and aggregation pathway for ACP formation which shows a differential lithium isotope effect, while other pathways do not allow for this effect. To expand upon this possibility, we note that measurements of the change in pH in similar solutions of KCl–$NaPO_4$–$CaCl_2$ show a pH-dependent shift in the change in protonation state of phosphates upon the addition of calcium (*SI Appendix*, Fig. S5), indicating that different molecular calcium phosphate species, for example calcium triphosphate vs. Posner clusters, are preferred at different levels of pH and/or supersaturation. At even higher pHs, HAp nucleation may occur by a classical pathway that has been found to be in competition with the pathway in Fig. 1 in certain solution conditions (31). We hypothesize that the mechanism underlying the observed lithium isotope effect depends upon a particular nucleation pathway and thus molecular calcium phosphate species, as will be discussed in later sections.

Lithium Acts on Early-Stage Calcium-Phosphate Nucleation

Having established a differential lithium isotope effect in a particular range of compositions in vitro, we designed experiments to investigate at what stage in the ACP formation pathway (Fig. 1) this effect manifests. Given that DLS is primarily sensitive to structures at several hundred nanometers in scale, any of the steps leading up to the formation of such large ACP aggregates (stage 4) could be involved in the isotope effect. Therefore, we tested the possibility that a lithium isotope effect could occur at each stage of the ACP aggregation process.

First, we consider whether stage I, before any calcium phosphate structures have formed, could be differentially impacted. Such an effect could arise, for example, from different local water structuring around atoms of the two lithium isotopes, or due to a direct lithium–phosphate interaction (we assume no significant lithium–calcium interactions given they are both positively charged). As noted, ^{6}Li and ^{7}Li have indistinguishable aqueous diffusion rates (42). This diffusion coefficient is proportional to the hydrodynamic diameter of the ions, which includes the bound water molecules around the ion. Thus, we expect no significant isotopic difference in the local water structuring.

To address the possibility of differential ionic lithium–phosphate interactions, we characterized solutions of lithium and phosphate using ^{31}P NMR before adding calcium. The resulting spectra (Fig. 4*A*) show nearly identical chemical shift and line width for phosphorus in the presence of ^{6}Li and ^{7}Li, indicating no significant difference in ionic lithium–phosphate chemistry. The small observed chemical shift difference of ~0.01 ppm is of the order typically seen for isotopes, given that their different masses will change equilibrium bond length and therefore electron density at the phosphorus nucleus (50). We conclude that the observed isotope effect is not likely to manifest during stage I of ACP aggregation.

To investigate the potential for an isotope effect on later stages of ACP aggregation, we first established whether lithium is incorporated into the resulting calcium phosphate phase in an isotope-dependent manner. ^{31}P NMR performed after calcium addition indicates a ^{31}P shift in line shift and line width compared to solutions containing no calcium (Fig. 4*A*), confirming that a new phase of calcium-phosphate forms which we identify as ACP.

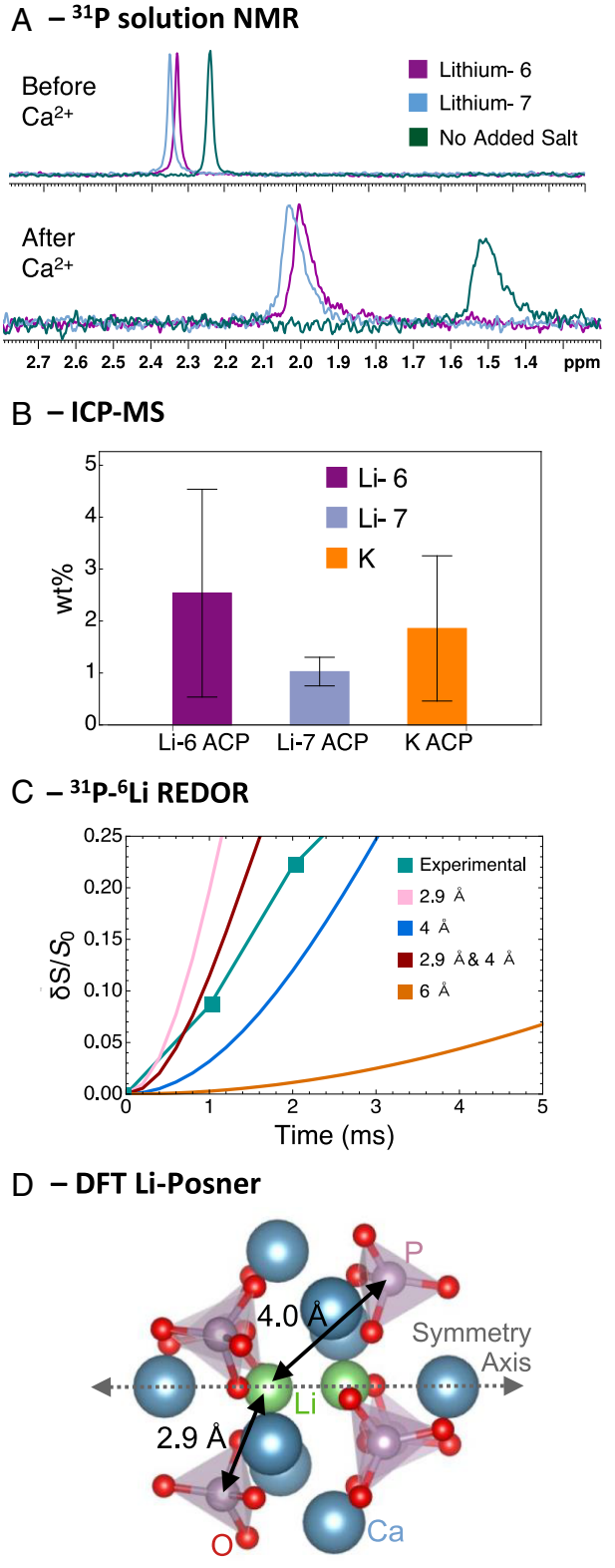

Fig. 4. ^{31}P NMR and ICP-MS confirm the incorporation of lithium into ACP phase. (*A*) ^{31}P NMR on LiCl–$NaPO_4$–$CaCl_2$ solutions shows similar chemical shift in the presence of ^{7}Li and ^{6}Li both before and after calcium addition, indicating no isotopic difference in phosphate–lithium interactions and similar incorporation of Li into ACP. (*B*) ICP-MS results on ACP synthesized in the presence of 250 mM ^{6}LiCl, ^{7}LiCl, or KCl demonstrate similar incorporation of Li isotopes into the ACP phase at ~1 wt% (error bars indicate SE across 10 independent trials). Potassium also incorporates at $\propto$ 1 wt%. (*C*) ssNMR REDOR on ^{31}P–^{6}Li coupling shows Li–P distances of $\leq$4 Å. A fit with an equal mix of 2.9 Å and 4 Å distances, based on DFT calculations for the geometry of a Posner molecule with two lithium atoms replacing the central calcium, shown in (*D*), shows agreement with the experimental curve.

The ^{31}P signal for ACP in the presence of both lithium isotopes were again similar in line width and position, suggesting that lithium incorporates into the calcium phosphate aggregates in an isotope-independent manner.

The incorporation of lithium into the calcium phosphate phase was confirmed using inductively coupled plasma mass spectrometry (ICP-MS). An ACP powder was synthesized as described in *Materials and Methods*, such that initial calcium phosphate nucleation conditions were identical to those measured in DLS. Therefore, if lithium is incorporated in this synthesized powder, then we would also expect it to be present in the soluble structures that we measure using DLS. ^{31}P and ^{6}Li spin counting experiments verified that this synthesized powder was ACP (47) and that there was no reprecipitated LiCl in the powder (*SI Appendix*, Fig. S6). ICP-MS traces for ACP powders synthesized in the presence of 250 mM $^{6}LiCl$ and $^{7}LiCl$ indicate that both isotopes were incorporated into the resulting phase at ∼1 wt% (Fig. 4*B*), with the large error bars resulting from difficulties in ablating the solid powders and mass-dependent transport through the apparatus. Assuming that ACP is ∝ 20 wt% water (51) and composed of a glass of Posner molecules of stoichiometry $Ca_9(PO_4)_6$, this concentration would correspond to approximately one lithium ion per Posner molecule, indicating that enough lithium may be incorporated to have a significant impact on Posner dynamics. Although such "doping" of ACP with lithium has not been reported previously in experiments, previous DFT calculations on Posner molecules indicated an energetic preference for two lithium ions to replace the central calcium ion (26), providing a potential explanation for the observed lithium incorporation.

Having established that lithium incorporates into ACP in an isotope independent manner, we consider whether later stages of ACP aggregation could be impacted by lithium addition in an isotope-dependent manner. For the aggregation of calcium phosphate particles (∼100 nm in diameter) into larger aggregates (several hundred nm to several microns), we expect that the colloidal aggregation of ACP particles in aqueous salt solution is dominated by Derjaguin–Landau–Verwey–Overbeek interactions, i.e., an interplay between short-range van der Waals attractions and longer-range electrostatic repulsion (52). Since the lithium isotopes have the same charge and electronic structure, neither of these forces should show a strong isotope dependence, so it is unlikely that the lithium isotope effect arises at this stage. We also observe that the calcium phosphate solid-state boundary shows no isotopic dependence (Fig. 3*A*), in agreement with the DLS results that show that there is no isotopic dependence of ACP size. We expect the concentration of metastable ACP particles to be primarily determined by the degree of supersaturation of calcium phosphate in solution, and so we infer that there does not appear to be a differential lithium isotope effect on stages III and IV of ACP aggregation.

Given the above arguments, neither the earliest (ionic) nor latest stages (colloidal aggregation) of ACP aggregation seem likely to be the source of the observed isotope effect. Therefore, we propose that it is during the formation and aggregation of nanoclusters (stage II) of ACP aggregation that the differential lithium isotope effect must be operative.

A Possible Mechanism for a Differential Isotope Effect

To understand a possible mechanism for the lithium isotope effect on calcium phosphate aggregation, we consider the physical differences between the properties of ^{6}Li and ^{7}Li ions within putative calcium phosphate molecular species (e.g., Posner molecules). Since the two isotopes of lithium have essentially identical electronic structure, this would presumably rule out any chemical differences in interactions between lithium isotopes, and their nearly identical diffusivities in water indicate similar dynamics in solution. However, the nuclear spin properties of ^{6}Li and ^{7}Li differ significantly. ^{6}Li is a spin-1 nucleus, although due to its small quadrupole moment, it is often considered an "honorary spin-1/2" nucleus, with a T_1 relaxation time on the order of minutes in water (53). On the other hand, ^{7}Li is a spin-3/2 nucleus, with a quadrupole moment two orders of magnitude greater than ^{6}Li, and a T_1 on the order of seconds in water (53). Therefore, we expect these two lithium isotopes could have significantly different spin coupling to the ^{31}P nuclei within the Posner molecule, and thus affect their aggregation dynamics, as will be expanded upon later.

To experimentally test whether lithium is proximal enough to phosphorus to have notable spin coupling between the two nuclei, we used the rotational-echo, double-resonance NMR (REDOR) sequence on an ACP powder synthesized in the presence of 250 mM ^{6}Li. Briefly, REDOR measure dipolar coupling between two heteronuclear spins, from which an interspin distance can be extracted (54). For these measurements, ^{6}Li was chosen in the preparation of ACP over ^{7}Li due to its significantly slower relaxation rate, which aids in data acquisition and analysis. However, given that solution NMR and ICP-MS results show similar level of incorporation of ^{6}Li and ^{7}Li into ACP, we expect the results on the ^{6}Li system to also provide insight into the ^{7}Li system.

While REDOR can be difficult to fit to extract precise distances when there is a dispersity of internuclei distances and multispin (≥3) effects, the early time REDOR buildup curve can still indicate the strongest dipolar couplings (and thus shortest distances) in the system. The early-time ^{31}P–^{6}Li REDOR curve (Fig. 4*C*) shows a measurable signal buildup that indicates significant ^{31}P–^{6}Li spin coupling and ^{31}P–^{6}Li distances on the scale of 3 to 4 Å (the REDOR curve for a 6 Å distance is also shown to illustrate that even slightly farther distances produce large differences in the observed signal). DFT calculations on a Posner molecule with two lithium ions replacing the central calcium ion yield lithium-phosphorus distances of 2.9 Å for three ^{31}P's and 4 Å for the other three ^{31}P's, and a REDOR model based on this distance distribution shows good agreement with the experimentally measured buildup curve. Regardless of specific distances, the close proximity of the two spins indicates a spin-coupling based mechanism for the differential isotope effect could be physically possible. Notably, DFT indicates that this lithium-doped Posner molecule maintains threefold symmetry within 0.05 Å, the importance of which is expanded upon below.

Colloidal aggregation can be theoretically described as a diffusion-reaction process by which—for the case of pair binding—individual particles encounter one another by diffusive transport and bind through intermolecular and surface forces. In the case of Posner molecules, calculations on the energy landscape for pair binding have found an energetically preferred orientation of pair binding in which Posner molecules have their C_3 axes antialigned (26). This suggests that there is significant coupling between the rate of pair binding to the orientational dynamics, and thus the relative angular orbital momentum states, of a binding pair of Posner molecules. This provides a potential link between colloidal aggregation and the ^{31}P states of Posner molecules, as follows.

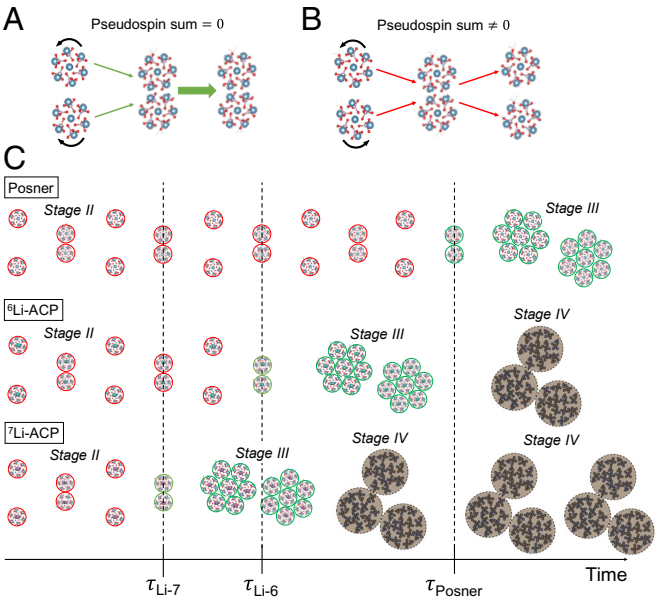

Fig. 5. An illustration of a potential mechanism for the impact of pseudospin on Posner molecule pair binding. (*A*) Two antialigned Posner molecules with total pseudospin of 0 are able to access a real wave function that is required for bonding. Black arrows indicate that the pseudospins are opposite in this case. (*B*) Two antialigned Posner molecules with nonzero total pseudospin (black arrows in the same direction) are unable to form a real wave function, thus bond formation cannot occur. (*C*) The pseudospin coherence time, τ, would be shorter for ^{7}Li-doped Posners compared to ^{6}Li-doped or undoped Posners. After a pseudospin restricted binding attempt, the pseudospin would decohere fastest for ^{7}Li Posners, allowing them to make a new projective measurement onto pseudospin and bind. These bound pairs can then aggregate into ACP colloids, resulting in a higher population of particles at the largest size in the presence of ^{7}Li as compared to ^{6}Li.

Within the framework of the quantum brain theory, the so-called quantum dynamical selection rule posits that the collective ^{31}P spin states within the Posner molecule function as a qutrit with a quantum number defined by the phase factor acquired during a symmetry-preserving rotation, which we call the "pseudospin" (27). Due to the Fermi statistics of the spin-$\frac{1}{2}$ phosphorus nuclei under this rotation, the orbital angular momentum (and rotational dynamics) of the molecule is then constrained by this pseudospin. In this way, only certain spin sectors (that sum to zero) are able to access a real wave function (and stop relative rotation between molecules) which is a requirement to form a chemical bond between pairs of Posner molecules (Fig. 5 *A* and *B*). In this way, the ^{31}P spin states of the Posner molecules are proposed to impact the apparent chemical reaction rates of Posner molecule pair-binding and, subsequently, downstream aggregation events in the aggregation of amorphous calcium phosphate. Note that while we focus on the Posner molecule here, quantum dynamical selection would hold for any calcium phosphate nanocluster with a threefold or greater symmetry axis, such as the molecular calcium phosphate cluster $Ca_6(PO_4)_4$, which has fourfold symmetry, that has been proposed to have longer spin coherence times than the Posner (55).

This proposal is difficult to test directly because NMR is unable to probe the collective spin state of a molecule, instead measuring an ensemble of spin states across all spins within a given chemical environment. However, we can still consider what measurable consequences the theory would have. These collective spin states will eventually decohere, in a sort of analog to the conventional T_2 relaxation rate for a single spin in NMR, allowing for previously precluded binding to occur. The rate of this decoherence will depend on the coupling of the spins within which the collective state is encoded (here ^{31}P) to the environment (including other spins within the molecule, such as lithium). Therefore, if two isotopes with different spins were to be incorporated into molecular clusters while preserving the molecular symmetry, one might expect the collective spin state lifetime to differ. In such a case, there might be an appreciable difference in pair-binding reaction rates between the two different isotopically doped species. This concept is shown schematically in Fig. 5*C*, comparing a typically composed Posner molecule with Posner molecules doped with ^{6}Li and ^{7}Li.

While this proposal is still speculative, it is currently difficult to put forward any other potential explanation for the observed experimental finding. Our ^{31}P NMR, ICP-MS, and phase mapping results rule out ionic interactions, differential incorporation, or solid phase behavior as potential causes for this isotope effect. As such, this highly unusual effect implies the need for an unconventional understanding of calcium phosphate aggregation. Regardless of the exact mechanism behind the observed isotope effect, the finding of an in vitro lithium isotope effect on ACP aggregation is an important step toward understanding the in vivo lithium isotope effects that have been observed in a wide range of biological systems.

Conclusion

We have presented evidence for a differential lithium isotope effect on the in vitro formation of amorphous calcium phosphate at biologically relevant conditions. DLS experiments showed that while the size of ACP formed is identical in the presence of ^{6}Li and ^{7}Li, certain conditions promote a measurable difference in scattering intensity that indicates a difference in the abundance of nanoscale ACP clusters. ^{31}P NMR measurements confirm the incorporation of both lithium isotopes into the ACP phase and indicate the presence of Li–P spin couplings, indicating the possibility that the observed isotopic effect may be due to differing nuclear spin interactions between ^{6}Li or ^{7}Li with ^{31}P. The reported isotopic effect could potentially be explained by a quantum-based condition for symmetric prenucleation molecular binding, where the spins of the two lithium isotopes differentially impact the probability of Posner binding during early nucleation events.

Our experiments suggest the existence of an in vitro differential lithium isotope effect, which has previously only been seen in biological systems. These results offer a potential physical mechanism for previously observed in vivo lithium isotope effects and are consistent with predictions by the Posner molecule–mediated quantum brain theory. Given these findings, we propose that additional investigations of differential isotope effects—for lithium and other elements—on mineralization processes be undertaken both in vivo and in vitro to expand our understanding of putative quantum phenomena in biological and abiotic systems.

Materials and Methods

All materials and methods are described in detail in *SI Appendix*.

Data, Materials, and Software Availability. All data and figures are available directly in the manuscript and/or *SI Appendix*.

ACKNOWLEDGMENTS. We would like to acknowledge Michel Gingras for a careful reading of the manuscript, as well as Tobias Fromme, Marshall Deline, Songi Han, and Zoya Leonenko for many useful discussions. Portions

of this work were used in the PhD thesis of J.S.S. This work was partially supported by the Heising-Simons Foundation (Award No. 2020-2427) and by Ionis Pharmaceuticals (Award No. PO 581247). Computational work utilized facilities purchased with funds from the NSF (CNS-1725797) and administered by the University of California, Santa Barbara Center for Scientific Computing (CSC). The CSC is supported by the California NanoSystems Institute and the Materials Research Laboratory, a National Science Foundation Materials Research Science and Engineering Centers (NSF DMR 2308708). This work also utilized MRL Shared Experimental Facilities supported by the MRSEC Program of the NSF under Award No. DMR 2308708; a member of the NSF-funded Materials Research Facilities Network (https://www.mrfn.org). This work utilized magnetic resonance instrumentation that was also supported in part by NSF Major Research Instrumentation Award, MRI-1920299.

Author affiliations: [a]Department of Physics, University of California, Santa Barbara, CA 93106; [b]Department of Chemistry, University of California, Santa Barbara, CA 93106; [c]Department of Materials, University of California, Santa Barbara, CA 93106; and [d]Department of Chemical Engineering, University of California, Santa Barbara, CA 93106

Author contributions: J.S.S., M.L.P., M.P.A.F., and M.E.H. designed research; J.S.S., M.L.P., M.S.N., L.R., and M.E.T. performed research; J.S.S., M.L.P., M.S.N., and M.E.H. analyzed data; and J.S.S., M.L.P., and M.E.H. wrote the paper.

1. P. O. Löwdin, Proton tunneling in DNA and its biological implications. *Rev. Mod. Phys.* **35**, 724–732 (1963).
2. A. Kohen, J. P. Klinman, Hydrogen tunneling in biology. *Chem. Biol.* **6**, R191–R198 (1999).
3. L. Turin, A spectroscopic mechanism for primary olfactory reception. *Chem. Senses* **21**, 773–791 (1996).
4. C. C. Gradinaru *et al*., An unusual pathway of excitation energy deactivation in carotenoids: Singlet-to-triplet conversion on an ultrafast timescale in a photosynthetic antenna. *Proc. Natl. Acad. Sci. U.S.A.* **98**, 2364–2369 (2001).
5. G. S. Engel *et al*., Evidence for wavelike energy transfer through quantum coherence in photosynthetic systems. *Nature* **446**, 782–786 (2007).
6. F. Fassioli, R. Dinshaw, P. C. Arpin, G. D. Scholes, Photosynthetic light harvesting: Excitons and coherence. *J. R. Soc. Interface.* **11**, 20130901 (2014).
7. W. Wiltschko, R. Wiltschko, Magnetic orientation and magnetoreception in birds and other animals. *J. Comp. Physiol. A.* **191**, 675–693 (2005).
8. H. Mouritsen, T. Ritz, Magnetoreception and its use in bird navigation. *Curr. Opin. Neurobiol.* **15**, 406–414 (2005).
9. C. T. Rodgers, P. J. Hore, Chemical magnetoreception in birds: The radical pair mechanism. *Proc. Natl. Acad. Sci. U.S.A.* **106**, 353–360 (2009).
10. M. P. A. Fisher, Quantum cognition: The possibility of processing with nuclear spins in the brain. *Ann. Phys.* **362**, 593–602 (2015).
11. J. Sechzer, K. Lieberman, G. Alexander, D. Weidman, P. Stokes, Aberrant parenting and delayed offspring development in rats exposed to lithium. *Biol. Psychiatry* **21**, 1258–1266 (1986).
12. A. Ettenberg *et al*., Differential effects of lithium isotopes in a ketamine-induced hyperactivity model of mania. *Pharmacol. Biochem. Behav.* **190**, 172875 (2020).
13. N. Li *et al*., Nuclear spin attenuates the anesthetic potency of xenon isotopes in mice: Implications for the mechanisms of anesthesia and consciousness. *Anesthesiology* **129**, 271–277 (2018).
14. M. Deline *et al*., Lithium affect mitochondrial amorphous calcium phosphate aggregation in a tissue and isotope dependent manner. *Front. Physiol.* **14**, 1200119 (2023).
15. J. D. Livingstone, M. J. Gingras, Z. Leonenko, M. A. Beazely, Search for lithium isotope effects in neuronal HT22 cells. *Biochem. Biophys. Rep.* **34**, 101461 (2023).
16. J. Smith, H. Zadeh Haghighi, D. Salahub, C. Simon, Radical pairs may play a role in xenon-induced general anesthesia. *Sci. Rep.* **11**, 6287 (2021).
17. H. Zadeh-Haghighi, C. Simon, Entangled radicals may explain lithium effects on hyperactivity. *Sci. Rep.* **11**, 12121 (2021).
18. N. Blumenthal, A. Posner, Hydroxyapatite: Mechanism of formation and properties. *Cal. Tis Res.* **13**, 235–243 (1973).
19. S. V. Dorozhkin, M. Epple, Biological and medical significance of calcium phosphates. *Angew. Chem. Int. Ed.* **41**, 3130–3146 (2002).
20. A. L. Lehninger, Mitochondria and calcium ion transport. *Biochem. J.* **119**, 129 (1970).
21. S. G. Wolf *et al*., 3D visualization of mitochondrial solid-phase calcium stores in whole cells. *eLife* **6**, e29929 (2017).
22. C. Pak, E. Eanes, B. Ruskin, Spontaneous precipitation of brushite in urine: Evidence that brushite is the nidus of renal stones originating as calcium phosphate. *Proc. Natl. Acad. Sci. U.S.A.* **68**, 1456–1460 (1971).
23. A. P. Evan *et al*., Crystal-associated nephropathy in patients with brushite nephrolithiasis. *Kidney Int.* **67**, 576–591 (2005).
24. D. Hirsch, R. Azoury, S. Sarig, H. S. Kruth, Colocalization of cholesterol and hydroxyapatite in human atherosclerotic lesions. *Calcif. Tissue Int.* **52**, 94–98 (1993).
25. J. S. Lee, J. D. Morrisett, Detection of hydroxyapatite in calcified cardiovascular tissues. *Atherosclerosis* **224**, 340–347 (2012).
26. M. W. Swift, C. G. Van de Walle, M. P. A. Fisher, Posner molecules: From atomic structure to nuclear spins. *Phys. Chem. Chem. Phys.* **20**, 12373–12380 (2018).
27. M. P. A. Fisher, L. Radzihovsky, Quantum indistinguishability in chemical reactions. *Proc. Natl. Acad. Sci. U.S.A.* **115**, E4551–E4558 (2018).
28. C. de P. Eduardo *et al*., Dentin decalcification during lithium treatment: Case report. *Spec. Care Dentist.* **33**, 91–95 (2013).
29. A. Dey *et al*., The role of prenucleation clusters in surface-induced calcium phosphate crystallization. *Nat. Mater.* **9**, 1010–1014 (2010).
30. W. J. Habraken *et al*., Ion-association complexes unite classical and non-classical theories for the biomimetic nucleation of calcium phosphate. *Nat. Commun.* **4**, 1–12 (2013).
31. K. He *et al*., Revealing nanoscale mineralization pathways of hydroxyapatite using in situ liquid cell transmission electron microscopy. *Sci. Adv.* **6**, eaaz7524 (2020).
32. E. M. M. Weber *et al*., Assessing the onset of calcium phosphate nucleation by hyperpolarized real-time NMR. *Anal. Chem.* **92**, 7666–7673 (2020).
33. F. Betts, A. Posner, An X-ray radial distribution study of amorphous calcium phosphate. *Mater. Res. Bull.* **9**, 353–360 (1974).
34. A. Oyane, K. Onuma, T. Kokubo, A. Ito, Clustering of calcium phosphate in the system $CaCl_2$–H_3PO_4–KCl–H_2O. *J. Phys. Chem. B* **103**, 8230–8235 (1999).
35. A. L. Boskey, A. S. Posner, Conversion of amorphous calcium phosphate to microcrystalline hydroxyapatite. A pH-dependent, solution-mediated, solid–solid conversion. *J. Phys. Chem.* **77**, 2313–2317 (1973).
36. F. Grases, M. Zelenková, O. Söhnel, Structure and formation mechanism of calcium phosphate concretions formed in simulated body fluid. *Urolithiasis* **42**, 9–16 (2014).
37. J. S. Straub *et al*., Phosphates form spectroscopically dark state assemblies in common aqueous solutions. *Proc. Natl. Acad. Sci. U.S.A.* **120**, e2206765120 (2023).
38. L. Wang, S. Li, E. Ruiz-Agudo, C. V. Putnis, A. Putnis, Posner's cluster revisited: Direct imaging of nucleation and growth of nanoscale calcium phosphate clusters at the calcite-water interface. *CrystEngComm* **14**, 6252–6256 (2012).
39. A. Lotsari, A. K. Rajasekharan, M. Halvarsson, M. Andersson, Transformation of amorphous calcium phosphate to bone-like apatite. *Nat. Commun.* **9**, 4170 (2018).
40. A. S. Posner, F. Betts, Synthetic amorphous calcium phosphate and its relation to bone mineral structure. *Acc. Chem. Res.* **8**, 273–281 (1975).
41. G. Mancardi, C. Tamargo, D. Tomasso, N. de Leeuw, Detection of Posner's clusters during calcium phosphate nucleation: A molecular dynamics study. *J. Mater. Chem. B* **5**, 7274–7284 (2017).
42. P. F. Renshaw, A diffusional contribution to lithium isotope effects. *Biol. Psychiatry* **22**, 73–78 (1987).
43. K. Onuma *et al*., Precipitation kinetics of hydroxyapatite revealed by the continuous-angle laser light-scattering technique. *J. Phys. Chem. B* **104**, 10563–10568 (2000).
44. J. R. de Bruyn *et al*., Dynamic light scattering study of inhibition of nucleation and growth of hydroxyapatite crystals by osteopontin. *PLoS ONE* **8**, 1–9 (2013).
45. V. Čadež *et al*., Amorphous calcium phosphate formation and aggregation process revealed by light scattering techniques. *Crystals* **8**, 254 (2018).
46. L. Wang, G. H. Nancollas, Calcium orthophosphates: Crystallization and dissolution. *Chem. Rev.* **108**, 4628–4669 (2008).
47. M. S. Nowotarski *et al*., Dynamic nuclear polarization enhanced multiple-quantum spin counting of molecular assemblies in vitrified solutions. *Phys. Chem. Lett.* **15**, 7084–7094 (2024).
48. G. Mie, Sättigungsstrom und stromkurve einer schlecht leitenden flüssigkeit. *Ann. Phys.* **331**, 597–614 (1908).
49. L. Rayleigh, On the scattering of light by spherical shells, and by complete spheres of periodic structure, when the refractivity is small. *Proc. R. Soc. Lond., Ser. A* **94**, 296–300 (1918).
50. C. J. Jameson, *Isotope Effects on Chemical Shifts and Coupling Constants* (John Wiley & Sons Ltd., 2007).
51. A. S. Posner, N. C. Blumenthal, A. L. Boskey, F. Betts, Synthetic analogue of bone mineral formation. *J. Dent. Res.* **54**, 88–93 (1975).
52. J. N. Israelachvili, *Intermolecular and Surface Forces* (Academic Press, London, UK/San Diego, CA, ed. 2, 1991), p. xxi, 450p.
53. M. Mohammadi, S. Benders, A. Jerschow, Nuclear magnetic resonance spin-lattice relaxation of lithium ions in aqueous solution by NMR and molecular dynamics. *J. Chem. Phys.* **153**, 184502 (2020).
54. T. Gullion, Introduction to rotational-echo, double-resonance NMR. *Concepts Magn. Reson.* **10**, 277–289 (1998).
55. S. Agarwal, D. R. Kattnig, C. D. Aiello, A. S. Banerjee, The biological qubit: Calcium phosphate dimers, not trimers. *J. Phys. Chem. Lett.* **14**, 2518–2525 (2023).